Chemistry & Biology, Vol. 12, 1201–1210, November, 2005, ©2005 Elsevier Ltd All rights reserved. DOI 10.1016/j.chembiol.2005.08.009

DNA and Non-DNA Targets in the Mechanism of Action of the Antitumor Drug Trabectedin

Marie-Hélène David-Cordonnier,[1] Consuelo Gajate,[2,3] Osvaldo Olmea,[4] William Laine,[1] Janis de la Iglesia-Vicente,[2] Carlos Perez,[4] Carmen Cuevas,[4] Gabriel Otero,[4] Ignacio Manzanares,[4] Christian Bailly,[1] and Faustino Mollinedo[2,*]

[1]INSERM U-524 et Laboratoire de Pharmacologie Antitumorale du Centre Oscar Lambret
IRCL
Lille 59045
France

[2]Centro de Investigación del Cáncer
Instituto de Biología Molecular y Celular del Cáncer
CSIC-Universidad de Salamanca
Campus Miguel de Unamuno
E-37007 Salamanca
Spain

[3]Unidad de Investigación
Hospital Universitario de Salamanca
Campus Miguel de Unamuno
E-37007 Salamanca
Spain

[4]PharmaMar
Avda. de los Reyes, 1
P.I. La Mina-Norte
E-28770 Colmenar Viejo
Madrid
Spain

Summary

We have analyzed the DNA binding properties of the antitumor agent trabectedin (ET-743, Yondelis) and different analogs, namely, ET-745, lacking the C21-hydroxyl group, and ET-637, ET-594, ET-637-OBu, with modifications at the trabectedin C domain, versus their effects on cell cycle, apoptosis, and gene expression. ET-745 failed to bind DNA, highlighting the importance of the C21-hydroxyl group for DNA binding. Analogs ranked trabectedin >> ET-637 ≈ ET-594 > ET-637-OBu >> ET-745 for their DNA binding capacity; ET-637 and ET-594 display very different biological activities. Drugs were clustered in three major groups showing high (trabectedin, ET-637), intermediate (ET-637-OBu), and low (ET-594, ET-745) cytotoxic activity and similar transcriptional profiling responses. C21-hydroxyl-deficient analogs of the above-mentioned compounds showed a dramatic decrease in biological activity. Our data suggest that trabectedin interacts with an additional non-DNA target to raise an effective antitumor response, and that this interaction is favored through trabectedin-DNA complexes.

Introduction

Ecteinascidins (ETs) are a group of antitumor alkaloids extracted from the mangrove Caribbean tunicate *Ecteinascidia turbinata* in the late 1960s. Among the various ETs, ET-743 (a.k.a. trabectedin) proved to be cytotoxic at very low doses in a wide variety of tumor cells. This marine compound, registered under the trade name of Yondelis (trabectedin), has a broad spectrum of anticancer activity in vivo (soft tissue sarcoma cells are particularly sensitive to its action [1]) and is currently under Phase II clinical investigation for treatment of soft tissue sarcoma; ovarian, breast, endometrial, prostate, non-small cell lung cancers; and pediatric sarcomas [2–5]. So far, the only well established target for ETs is DNA. Trabectedin binds covalently to guanine residues in the minor groove of the DNA double helix to bend the molecule toward the major groove [6, 7]. At micromolar concentrations, trabectedin has also been shown to inhibit topoisomerase I [8] and a number of transcription factors, including nuclear transcription factor NF-Y [9], and has been shown to induce microtubule disorganization [10]. However, these effects are considered unlikely to be relevant to the mechanism of action of trabectedin, as they are evidenced at drug concentrations that exceed pharmacologically active concentrations (nM range) by a factor of 100 or higher [11–13]. The formation of ternary complexes of drug, DNA, and a nucleotide excision-repair protein that lead to DNA single-strand breaks in transcribed genes, which, in turn, result in eventual cell death, has been proposed as the major mechanism of trabectedin action [2, 14, 15]. The antitumor activity of trabectedin is achieved through two major dose-dependent actions on cancer cells: (1) transcription-dependent growth arrest with an accumulation of cells in G_2/M when used at a concentration of 1–10 nM, and (2) transcription-independent apoptosis when used at a concentration of 10–100 nM [16]. These cytostatic and proapoptotic activities of trabectedin result from the activation of two different signaling pathways [16].

Here, we investigate whether the DNA binding activity of trabectedin plays a role in the biological actions of this drug by analyzing the DNA binding features as well as the cytostatic, proapoptotic, and transcriptional profiling activities of a number of structurally related trabectedin analogs, ET-594, ET-637, ET-637-OBu, and ET-745 (Figure 1). Structure-activity relationship (SAR) studies in the ET series have been limited so far, mainly because of the small amount and low chemical diversity of analogs biosynthetically produced. However, the recently described synthesis of trabectedin [17, 18] and novel biosynthetic procedures have allowed for the production of different trabectedin analogs; therefore, more detailed SAR studies can be established [19]. The complex structure of trabectedin is usually deconvoluted into three parts. Subunits A and B represent the two tetrahydroisoquinoline rings that are fused into a monobridged pentacyclic skeleton. A third tetrahydroisoquinoline ring (subunit C) is linked to the A-B core via a ten membered lactone bridge through a benzylic sulfide linkage. Trabectedin binds to the minor groove of DNA to establish a covalent link to the exocyclic 2-amino group of guanine residues [6, 20]. The

*Correspondence: fmollin@usal.es

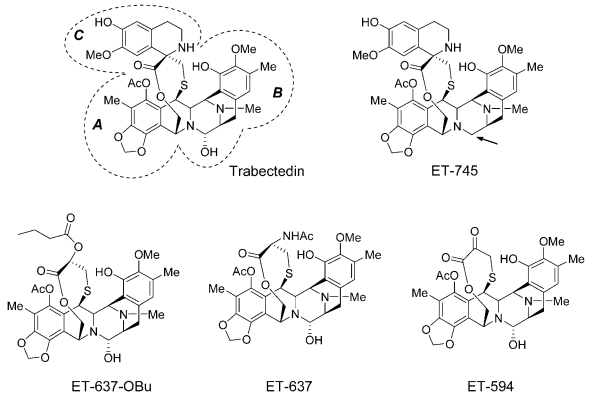

Figure 1. Structures of Trabectedin and Analogs

The three domains, A-B-C, of the trabectedin molecule are depicted. Compound ET-745 lacks the reactive C21-OH group (arrow), and compounds ET-637-OBu, ET-637, and ET-594 are modified at the C domain.

bonding reaction involves the carbinolamine functional group (N2-C21-OH). NMR and modeling studies have revealed that the crosslinking of DNA by trabectedin places the A and B subunits deep into the minor groove on the 5′ and 3′ sides, respectively, of the alkylated G, while the C subunit protrudes outside of the groove and shows little contact with DNA [21, 22]. This C subunit is perpendicularly oriented above the A-B core in the DNA minor groove and may serve as a hook for trapping proteins surrounding the drug-DNA complex. It may also play an indirect role in DNA recognition by constraining the architecture of the A-B skeleton and therefore influencing the dynamics of the drug/DNA interaction. However, the role of this portion of the trabectedin molecule remains unclear, and we address this issue here by using C-modified analogs. The compounds studied here include ET-745, which just lacks the key C21-hydroxyl group. The absence of the carbinolamine function is expected to prevent the drug from alkylating DNA. This analog is thus a good control by which to study binding versus bonding to DNA. Three additional compounds tested here share a common structural characteristic, namely, the loss of the tetrahydroisoquinoline C subunit that is replaced with an N-acetyl group (ET-637), a propionate ester (ET-637-OBu), or a keto function (ET-594). These three compounds thus provide excellent molecular tools by which to dissect the role of the C subunit of trabectedin in DNA recognition and guanine alkylation, and in the ensuing biological activities, including cell cycle arrest, apoptosis, and gene profiling (transcriptome) activity.

Results

DNA Binding Properties of Distinct Trabectedin Analogs

The interaction of trabectedin and its analogs with DNA was investigated by using gel shift and footprinting assays to compare the extent of binding and sequence selectivity. The compounds were incubated with a 2900 bp DNA restriction fragment for 1 hr, and samples were loaded on 1% agarose gels. As shown in Figure 2A, trabectedin strongly reduced the electrophoretic mobility

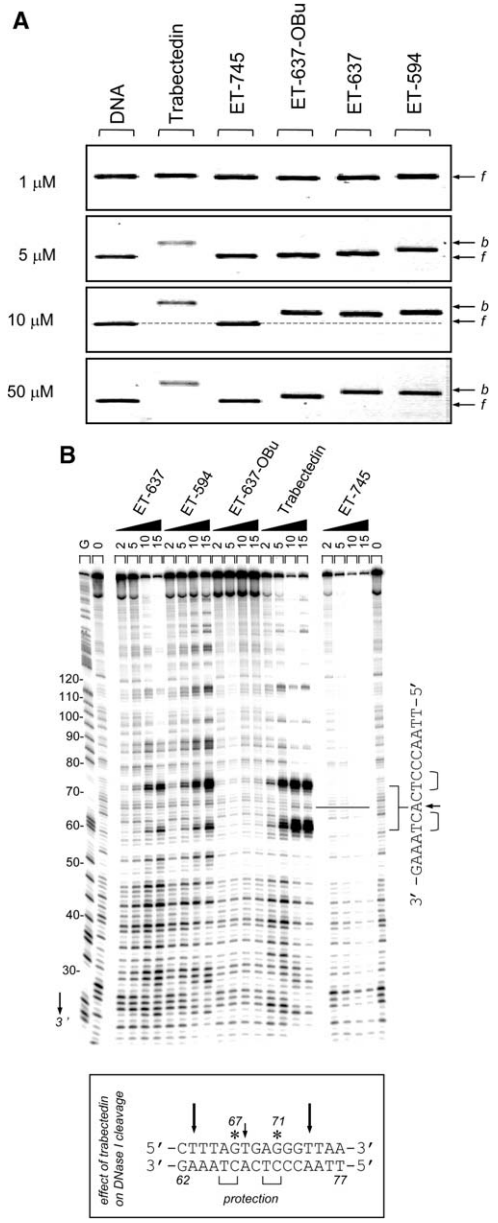

Figure 2. DNA Binding Capacity of Different Trabectedin Analogs

(A) Gel shift assay showing covalent binding of ET compounds (1–50 μM each) to a 2900 bp DNA fragment. The control lane (DNA) contained no drug. Symbols "*f*" and "*b*" refer to the free and drug bound DNA species, respectively.

(B) Sequence-selective binding by DNase I footprinting assays in a 265 bp fragment. (Upper) DNase I footprinting with a 265 bp restriction fragment in the presence of graded drug concentrations (in μM). Control lanes (0) contained no drug. Guanine-specific sequence markers obtained by treatment of the DNA with dimethylsulfate followed by piperidine were run in the lanes marked "G." The numbers on the left side of the gel refer to the standard numbering scheme for the nucleotide sequence of the DNA fragment. (Lower) The inset depicts the effect of trabectedin on DNase I cleavage at the 62–77 region from which the 16 bp oligonucleotide was derived. The drug stimulates DNA cleavage at the sites pointed out by arrows and protect the two juxtaposed AG/CT steps. The reactive guanines G67 and G71 are indicated by an asterisk.

of the DNA, whereas the analogs showed variable effects. ET-745 completely failed to reduce the mobility of DNA, even when tested at a concentration as high as 50 μM. The other analogs induced DNA retardation, but they were less potent than trabectedin. Assuming that the extent of gel retardation is proportional to the affinity of the drug for DNA and/or their DNA alkylation potential, the drugs rank in the order: trabectedin >> ET-637 ≈ ET-594 > ET-637-OBu >> ET-745. The level of gel retardation could reflect the putative DNA alkylation potential of the drugs because noncovalent DNA binding drugs generally do not induce such a pronounced effect on DNA migration during electrophoresis. In support of this view, we found that ethanol precipitation of samples to dissociate free drug from bound drug had no effect on gel retardation; trabectedin-DNA complexes, precipitated or not with ethanol, migrated at the same positions (data not shown), suggesting that gel shifts reflected covalent binding to DNA. The above-described gel shift data agreed with footprinting data (see below), and, therefore, the two methods tend to validate the following conclusions: (1) ET-745 does not bind to DNA, (2) ET-637 and ET-594 display similar potency in terms of DNA binding, and (3) trabectedin exhibits superior DNA binding properties compared to the analogs.

Similar gel shift experiments were performed with two other DNA fragments to confirm the previous observations in different DNA sequence contexts and to improve the resolution of the DNA binding study, up to the nucleotide level. On the one hand, we used a radiolabeled 56 bp restriction fragment obtained upon digestion of the plasmid pDB293-2 with BamHI and HindIII. The results obtained with this DNA substrate were consistent with those obtained with the long fragment. The electrophoretic mobility of this DNA was not affected by ET-745, whereas the other compounds showed a dose-dependent effect (data not shown). On the other hand, a short 16 bp oligonucleotide containing two high-affinity binding sites for trabectedin was selected from footprinting experiments (Figure 2B) and was used in subsequent gel shift assays. A 265 bp fragment showed a strong binding sequence for trabectidin and analogs ET-637 and ET-594 around nucleotide positions 60–70, with prominent sites of DNase I-enhanced cleavage flanking the binding sequence (Figure 2B). ET-745 did not show any sign of binding to DNA, whereas the other compounds clearly interacted with this target sequence (data not shown). This short 16 bp oligonucleotide, containing only two juxtaposed binding sites (Figure 2B), was used for melting temperature (*Tm*) experiments to study the drug effects on the duplex stability of the DNA. Under our experimental conditions, the melting temperature of the oligonucleotide was 33ºC, and a very strong duplex stabilizing effect was observed in the presence of trabectedin, with a ΔTm ($Tm^{\text{drug-DNA complex}} - Tm^{\text{DNA alone}}$) of up to 32ºC at a drug/DNA-nucleotide ratio of 0.1 (Figure 3A). The ΔTm values dropped with the analogs ET-637, ET-594, and ET-637-Obu, and this is consistent with their reduced DNA binding capacity (Figure 3B). ET-745 showed no effect on the melting temperature of DNA, further supporting its inability to alkylate DNA. Similar *Tm* data were obtained with DNA from calf thymus (data not shown).

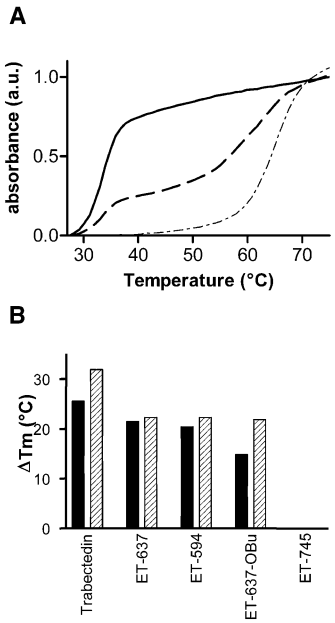

Figure 3. Effect of Trabectedin Analogs in DNA Thermal Denaturation

(A) Thermal denaturation curves for the 16 bp oligonucleotide (5′-CTTTAGTGAGGGTTAA-3′·5′-TTAACCCTCACTAAAG-3′, 20 μM in bases), derived from Figure 2B, in the absence (solid line) and presence of trabectedin at a drug-DNA (nucleotide) ratio of 0.1 (dotted line) and 0.05 (dashed line).

(B) Variation in melting temperature (ΔTm) for the different drugs at two drug-DNA(nucleotide) ratios, 0.1 (hatched bars) and 0.05 (black bars). ET-745 shows no binding to DNA, and, therefore, ΔTm is 0.

Sequence Selectivity in the DNA Binding Properties of Distinct Trabectedin Analogs

It could be argued that the lower extent of binding seen with the trabectedin analogs is not due to a reduced binding capacity, but to a modified sequence selectivity. Trabectedin has been previously reported to bind best to sequences containing 5′-AGC-3′ triplets compared to 5′-AGT-3′ triplets [7]. To investigate the sequence selectivity profile of the analogs, two types of experiments were performed. First, we used a gel shift assay employing a battery of 15-mer oligonucleotides having a common 5′-ATAATAXXXATAATA-3′/3′-TATTATYYYTATTAT-5′ motif and only differing by the nature of the central XXX/YYY triplet. Second, the sequence preference was investigated by means of DNase I footprinting to localize drug binding sites on long DNA fragments.

Gel shift assays performed with the XXX/YYY model system included the central triplet motifs AGA/TCT, CGA/TCG, GGA/TCC, GGC/GCC, CGG/CCG, GCG/CGC, or GGG/CCC. Representative gels are shown in Figure 4A, and the intensity of the band corresponding to the drug-DNA complex (bound) was compared to that of the unbound DNA (free). For trabectedin, the target oligonucleotides can be divided into four categories according to the level of binding: high (>40% bound: GGC/GCC and CGG/CCG), medium (20%–40% bound: GGA/TCC, GGG/CCC, GCG/CGC), low (5%–20% bound: AGA/TCT), and poor binding (<5% bound: CGA/TCG). These observations are consistent with the known sequence preference of trabectedin [6]. ET-745 showed

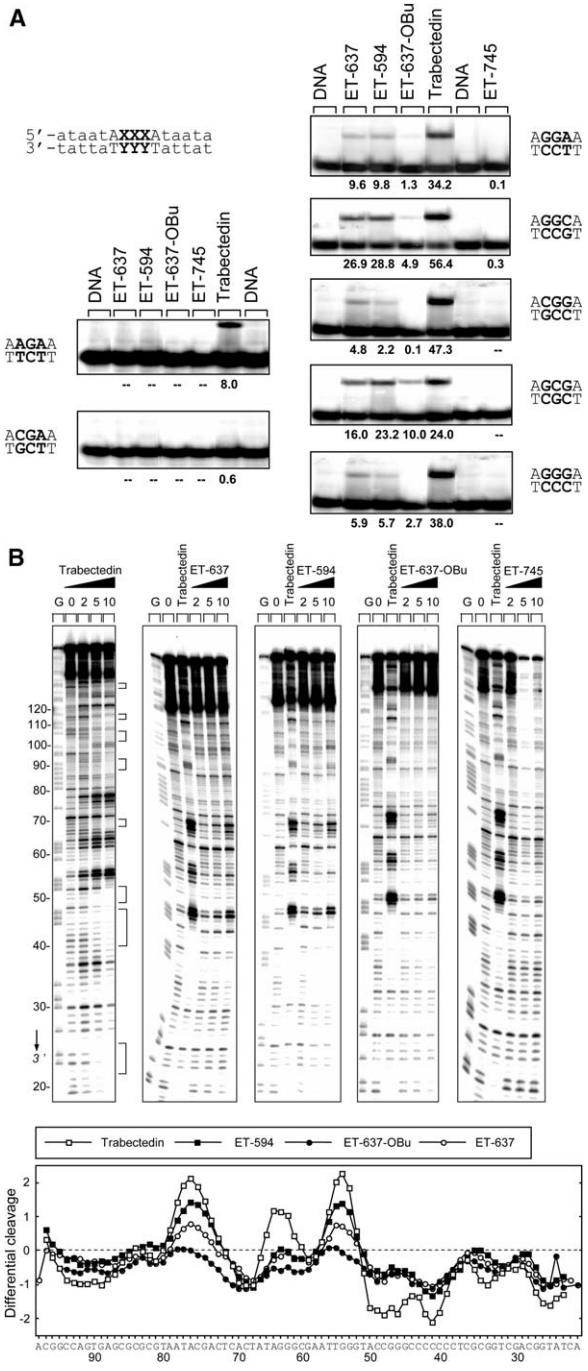

Figure 4. DNA Sequence Selectivity in the Binding of Different Trabectedin Analogs to DNA

(A) Gel shift assays for the binding of trabectedin and analogs to a series of 15 bp oligonucleotides containing a central triplet motif of variable sequence. Band intensities were quantified by densitometry, and the average values from three independent experiments are shown below each panel. –, no significant binding.

(B) Sequence-selective binding by DNase I footprinting assays in a 176 bp fragment. (Upper) DNase I footprinting in the presence of graded drug concentrations (in μM). Control tracks (0) contained no drug. Guanine-specific sequence markers were run in the lanes marked "G." The numbers on the left side of the gels refer to the standard numbering scheme for the nucleotide sequence of the DNA fragment. Square brackets indicate the positions of inhibition of DNase I cutting in the presence of the drugs. (Lower) Differential cleavage plots comparing the susceptibility of the 176 bp fragment to DNase I cutting in the presence of the different drugs (10 μM each). Negative values correspond to a ligand-protected site, and positive values represent enhanced cleavage. Vertical scales are in units of ln(fa) − ln(fc), where fa is the fractional cleavage at any bond in the presence of the drug, and fc is the fractional cleavage of the same bond in the control, given closely similar extents of overall digestion. Only the region of the restriction fragment analyzed by densitometry is shown.

almost no binding to any of the target oligonucleotides. ET-637 and ET-594 were found to bind much more weakly than trabectedin, and these two compounds behave similarly. In this gel shift assay, as well as in the footprinting assay (see below), these two analogs lacking the C subunit of trabectedin exhibited similar profiles of DNA recognition. They both showed good binding to the GGC/GCC- and GCG/CGC-containing oligonucleotides and failed to bind to AGA/TCT or CGA/TCG. The profile of ET-637-OBu is reminiscent of that of ET-637 and ET-594, but its overall affinity is further reduced.

DNase I footprinting experiments were carried out with two pieces of DNA: a 265-mer and a 176-mer restriction fragment. In both cases, the DNA substrate was 3′ end radiolabeled and subjected to limited cleavage by the endonuclease DNase I in the presence of increasing concentrations of the ET compounds. The products of degradation are then resolved by denaturing gel electrophoresis. Typical gels are shown in Figure 4B for the 176-mer and Figure 2B for the 265-mer. Trabectedin strongly affects the cleavage of DNA by the enzyme. With both fragments, the drug induced a pronounced dose-dependent increase in DNase I cleavage at several sites, such as around nucleotide positions 62 and 77 for the 265-mer (Figure 2B) and 55, 64, and 77 for the 176-mer (Figure 4B). Adjoining these sites, there were regions in which the cleavage by the enzyme was reduced or inhibited, and these regions corresponded to the drug binding sites (Figure 4B). The sites of enhanced cleavage were particularly intense and unusual for such a low-molecular weight compound. Two independent effects might contribute to the cleavage enhancement: redistribution of the enzyme at sites not occupied by the bound drug molecules (the mass action effect), and drug-induced structural changes of the DNA helix rendering the double helix more susceptible to cutting by the enzyme. In the present case, attribution of enhanced cleavage by DNase I to a mass action effect is implausible because it would lead to a general increase in cleavage. Thus, drug-induced structural changes are the only plausible explanation. In this regard, trabectedin induces DNA bending and a widening of the DNA minor groove, which could facilitate cleavage by the enzyme at locations surrounding the drug binding sites [7]. Whatever the exact origin of these enhancement sites is, they are very useful for comparing the extent of binding of the analogs. The sites of enhanced cleavage are much less pronounced with ET-637 and ET-594, and they are virtually absent with ET-637-OBu, compared to trabectedin. With the 265-mer fragment, a detailed analysis of the region between nucleotide positions 62–77 indicated that trabectedin, and to a lesser extent its analogs, protect the two juxtaposed 5′-AG-3′ steps from DNase I

Table 1. Dose Response and Time Course of the Effects of Trabectedin Analogs on Cell Cycle in HL-60 Cells

		Treatment							
		24 hr				48 hr			
Drug	M	Sub-G_1	G_0/G_1	S	G_2/M	Sub-G_1	G_0/G_1	S	G_2/M
Control	—	1.8 ± 0.7	57.0 ± 5.1	16.6 ± 1.8	24.6 ± 2.9	2.1 ± 0.7	59.5 ± 5.3	14.7 ± 2.4	23.7 ± 3.2
Trabectedin	10^{-7}	**58.2 ± 5.2**	24.1 ± 2.8	14.5 ± 1.9	3.2 ± 0.3	**90.2 ± 2.2**	5.8 ± 1.9	2.9 ± 0.3	1.1 ± 0.1
	10^{-8}	**49.3 ± 4.7**	26.4 ± 2.3	13.2 ± 1.3	11.1 ± 1.0	**85.6 ± 3.2**	9.4 ± 2.3	3.2 ± 0.3	1.8 ± 0.7
	10^{-9}	1.9 ± 0.2	26.1 ± 3.0	13.1 ± 1.9	**58.9 ± 6.0**	4.5 ± 0.4	20.3 ± 3.8	5.8 ± 1.2	**69.4 ± 5.1**
ET-637	10^{-7}	**56.3 ± 5.3**	25.6 ± 3.7	13.8 ± 1.8	4.3 ± 0.5	**89.1 ± 2.1**	6.9 ± 1.3	2.8 ± 0.7	1.2 ± 0.1
	10^{-8}	**48.6 ± 4.5**	27.1 ± 2.2	11.7 ± 1.2	12.6 ± 1.2	**83.4 ± 3.4**	10.6 ± 2.0	3.1 ± 0.8	2.9 ± 0.6
	10^{-9}	1.8 ± 0.2	25.3 ± 3.1	16.2 ± 2.7	**56.7 ± 5.3**	4.4 ± 0.4	22.1 ± 3.0	8.2 ± 1.7	**65.3 ± 5.1**
ET-637-OBu	10^{-7}	**47.6 ± 4.5**	28.7 ± 3.0	14.9 ± 1.3	8.8 ± 0.9	**86.2 ± 3.2**	9.8 ± 2.2	2.5 ± 0.8	1.5 ± 0.2
	10^{-8}	6.7 ± 0.9	16.9 ± 2.6	8.9 ± 1.9	**67.5 ± 5.1**	**26.8 ± 2.3**	19.2 ± 1.8	10.7 ± 1.0	**43.3 ± 3.1**
	10^{-9}	2.3 ± 0.2	53 ± 5.0	15.3 ± 2.4	**29.4 ± 3.0**	2.4 ± 0.3	47.3 ± 4.5	17.1 ± 1.5	**33.2 ± 3.2**
ET-594	10^{-7}	**48.3 ± 4.1**	28.2 ± 1.9	13.8 ± 1.2	9.7 ± 0.8	**85.0 ± 4.1**	7.9 ± 2.1	4.2 ± 1.2	2.9 ± 0.8
	10^{-8}	1.5 ± 0.2	42 ± 3.6	18.2 ± 1.6	**38.3 ± 3.6**	**10.3 ± 1.0**	50.8 ± 4.1	14.5 ± 1.3	24.4 ± 2.2
	10^{-9}	1.4 ± 0.2	55.5 ± 4.7	17.5 ± 1.5	25.6 ± 2.7	3.4 ± 0.3	55.4 ± 4.3	18.5 ± 2.0	22.7 ± 2.4
ET-745	10^{-7}	2.1 ± 0.2	46.5 ± 4.2	15.6 ± 1.3	**35.8 ± 3.4**	**18.3 ± 1.6**	49.4 ± 4.3	10.1 ± 1.0	22.2 ± 1.7
	10^{-8}	2.0 ± 0.2	56.3 ± 5.3	15.2 ± 1.3	26.5 ± 2.3	6.8 ± 0.9	60.1 ± 5.1	9.9 ± 1.8	23.2 ± 2.5
	10^{-9}	1.9 ± 0.2	60.1 ± 5.6	11.9 ± 1.0	26.1 ± 2.6	2.8 ± 0.5	59.6 ± 4.3	12.6 ± 1.8	25.0 ± 2.9

HL-60 cells were incubated with the indicated concentrations of the distinct trabectedin analogs for 24 and 48 hr, and the proportion of cells in each phase of the cell cycle was quantitated by flow cytometry. Cells in the sub-G_1 region represent apoptotic cells. Untreated control cells were run in parallel. Most relevant increases in sub-G_1 and G_2/M are labeled in bold. Data are shown as means ± SD of three independent experiments.

cleavage and strongly stimulate cutting at the flanking sites. The drug apparently reacted with the G67 and G71 residues (Figure 2B). With the 176-mer fragment, the differential cleavage plots (obtained from the densitometric analysis of the gels) indicate that the drugs bind preferentially to several GC-rich sequences, such as the exclusively GC sequence between positions 40 and 50. Here again, the analogs essentially recognize the same sites as trabectedin, but with a reduced affinity, and this is consistent with the above-mentioned *Tm* and gel shift data.

Effects of the Distinct Trabectedin Analogs on Cell Cycle and Apoptosis

Because trabectedin exerts two major biological effects on tumor cells, namely, cell cycle arrest and apoptosis [16], which account for the antitumor action of the drug, we next investigated the capacity of the above-described trabectedin analogs to promote cell cycle arrest and apoptosis in a human leukemic cell line (HL-60 acute myeloid leukemia cells) and two human solid tumor cell lines (HeLa cervix cancer cells and A459 lung cancer cells) to draw general conclusions about cancer cells. Surprisingly, we found that the biological activity of the above-described trabectedin analogs did not match their respective DNA binding abilities. Trabectedin induces a direct apoptotic response at 10 and 100 nM, whereas it arrests cells at G_2/M at at 1 nM concentration, eventually leading to cell death [16]. As shown in Table 1, for HL-60 cells, trabectedin and ET-637 showed a practically identical biological behavior, whereas ET-594, which displayed almost identical DNA binding properties to ET-637, was rather inactive at low concentrations (1 nM). ET-594 promoted an apoptotic response only at high doses (100 nM), and it exerted a weak cell cycle arrest effect at 10 nM. ET-745 was largely inactive, and only some weak cell cycle and apoptotic responses were achieved after protracted incubations with high drug concentrations (100 nM). ET-637-OBu showed an intermediate cytotoxic activity, lower than ET-637 and higher than ET-594 (Table 1). Similar results were obtained with HeLa cells and A459 cells (data not shown). Although there was some variability regarding the relative drug dose-response profiles to achieve cell cycle arrest and apoptosis when using distinct cell lines (data not shown), we found that all of the various compounds assayed were able to induce both cell cycle arrest and apoptosis. Thus, trabectedin and ET-637 promoted a direct apoptotic response in HL-60 and HeLa cells when used at a 10 or 100 nM concentration, and they also promoted a strong cell cycle arrest at G_2/M that eventually led to apoptosis when used at 1 nM (Table 1, and data not shown). However, ET-637-OBu induced both a direct apoptotic response and cell cycle-mediated apoptosis when used at a concentration of 10 nM in the solid tumor cell lines (data not shown), and it mostly induced G_2/M arrest followed by apoptosis in HL-60 cells (Table 1). ET-594 required 10 nM (in HL-60 and HeLa cells) and 100 nM (in A549 cells) concentrations to arrest cells in G_2/M. ET-745 required 100 nM doses to arrest cells at G_2/M in HL-60 and HeLa cells (Table 1, and data not shown). Although both cytostatic and apoptotic effects were observed in all three of the human tumor cell lines assayed, lung carcinoma A549 cells were more resistant, and higher drug doses were required to achieve similar biological effects to those detected in HL-60 and HeLa cells. This suggests that the target(s) of trabectedin is(are) present in the three cell lines studied here, but the signaling pathways set off by the target(s) seem to be more preponderant in some cells than in others, leading to a variable response among the distinct cell lines. Thus, cell type-specific downstream signaling events could affect the final outcome of trabectedin action. Overall, the biological data indicate that the drugs rank in the order trabectedin ≈ ET-637 > ET-637-OBu >> ET-594 > ET-745 for their capacity to induce dose-dependent cell cycle arrest and apoptosis.

Effects of the Distinct Trabectedin Analogs on JNK and Caspase-3 Activation

Because trabectedin-induced apoptosis involves c-Jun NH_2-terminal kinase (JNK) and caspase-3 activation [16], we next examined the effect of the distinct trabectedin analogs on these biochemical processes; assayed the presence of phospho-JNK, through the use of a monoclonal antibody specific for the phosphorylated forms of JNK1/2; and assayed cleavage of the typical caspase-3 substrate poly(ADP-ribose) polymerase (PARP), by using a polyclonal antibody that detected both the 116 kDa intact form and the 85 kDa cleaved form of PARP. The ability of the distinct trabectedin analogs to activate JNK and caspase-3 followed the order trabectedin $\approx$ ET-637 > ET-637-OBu >> ET-594 $\geq$ ET-745 (Figures 5A and 5B). This order is in good correlation with their relative effects on cell cycle arrest and apoptosis. β-actin was used as an internal control; there are equivalent protein amounts in each lane of the gels shown in Figures 5A and 5B (data not shown). On the other hand, neither trabectedin nor any of its analogs herein studied induced extracellular signal-regulated kinase (ERK) activation, assessed by the lack of any increase in the basal level of phospho-ERK (data not shown). In addition, neither trabectedin nor any of its analogs induced any change in the protein level of JNK or ERK (data not shown).

Relative Changes in Gene Expression Induced by Distinct Trabectedin Analogs in Tumor Cells

We next investigated the effects of the trabectedin analogs on gene expression by using oligonucleotide arrays. A549 cells were treated with the different trabectedin analogs (3 nM), and their respective actions on gene expression were compared to those of untreated cells (Figure 5C). At this low concentration, the drug cytotoxic action was transcription dependent [16]. A comparison of the overall transcriptional changes induced by the distinct analogs revealed that the distinct compounds could be clustered into three groups, according to their similarities on the respective induced gene expression profiles, namely: (1) trabectedin and ET-637; (2) ET-637-OBu; and (3) ET-594 and ET-745. Interestingly, this correlated well with the respective biological activities of the trabectedin analogs. A remarkable result from these microarray analyses was that the biologically active compounds trabectedin, ET-637, and ET-637-OBu affected the expression of genes related to DNA damage, whereas the rather inactive analogs ET-594 and ET-745 did not. In this regard, the three biologically active compounds upregulated 1.8- to 2.6-fold the DNA repair genes *XPC* (xeroderma pigmentosum complementation group C), *GADD45* (growth arrest and DNA-damage-inducible), and *DDB2* (damaged-DNA binding protein 2), whereas no effect was observed with the inactive analogs; these changes have been confirmed by quantitative RT-PCR (data not shown).

Analogs Lacking the C21-OH Group Show Reduced Biological Activity

Our data indicate that ET-745, with a molecular structure similar to that of trabectedin, but lacking the C21-OH (Figure 1), fails to bind to DNA and shows a very reduced cytotoxic activity compared to trabectedin.

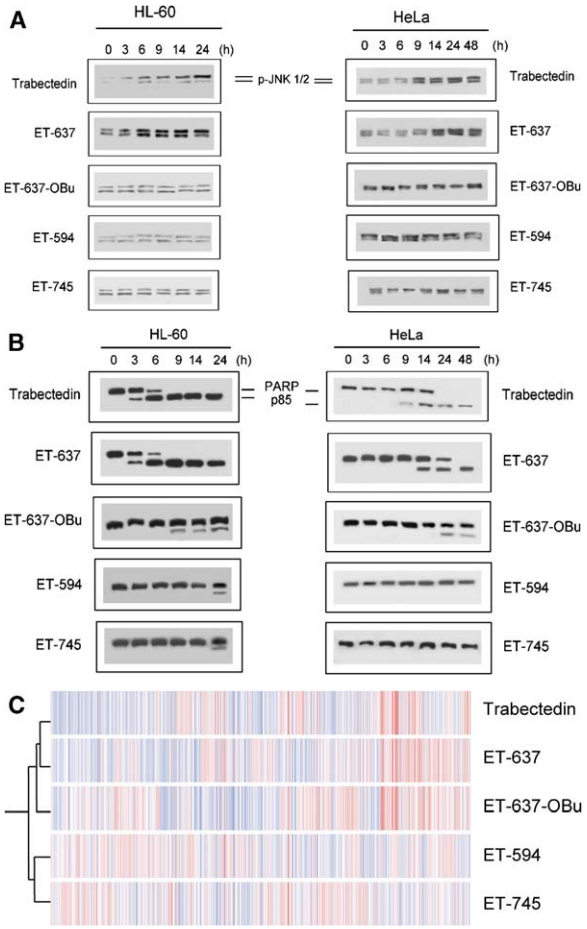

Figure 5. Effect of Different Trabectedin Analogs on Biochemical Apoptotic Parameters and Gene Expression

(A and B) HL-60 and HeLa cells were incubated with the distinct trabectedin analogs at 10 nM for the times indicated and then analyzed for (A) JNK activation and (B) PARP degradation by immunoblotting with anti-phospho-JNK and anti-PARP antibodies, respectively. The migration positions of (A) phospho-JNK1/2 as well as of full-length PARP and its cleavage product p85 are indicated. Experiments shown are representative of the three that were performed.

(C) Hierarchical clustering of gene expression data during treatment of A549 cells with distinct trabectedin analogs. A549 cells were treated with the indicated compounds (3 nM) for 8 hr, and then processed for gene microarray analysis. Columns represent individual genes, and rows represent the cell treatment with the indicated drugs. The color of each square represents the median-polished normalized ratio of gene expression in A549 cells treated with the indicated drug relative to untreated A549 cells. Red indicates gene expression above the median; blue, below the median; white, equal to median. Branch lengths of the dendogram show the degree of similarity between the gene expression profiles induced by each drug.

We then synthesized the C21-OH-deficient analogs of ET-637, ET-637-OBu, and ET-594, named ET-639, ET-637-OBu-C21(H), and ET-596, respectively, and analyzed their cytotoxic activities. As shown in Table 2, the lack of the C21-OH group drastically reduced the cytotoxic activity of the parental drugs to similar values in all three of the human tumor cell lines assayed. The less active the parental compound is, the less effect the lack of the C21-OH group on cytotoxicity has. In fact, the

Table 2. Antiproliferative Activity of Trabectedin-Related Compounds

Compound	C-21	Cell Line		
		HL-60	HeLa	A549
Trabectedin	OH	$1.2 \pm 0.2 \times 10^{-9}$	$2.3 \pm 0.3 \times 10^{-9}$	$3.4 \pm 0.6 \times 10^{-8}$
ET-745	H	$2.2 \pm 0.2 \times 10^{-6}$	$2.6 \pm 0.2 \times 10^{-6}$	$7.1 \pm 0.7 \times 10^{-6}$
ET-637	OH	$2.4 \pm 0.3 \times 10^{-9}$	$3.6 \pm 0.4 \times 10^{-9}$	$5.2 \pm 0.6 \times 10^{-8}$
ET-639	H	$2.3 \pm 0.2 \times 10^{-5}$	$3.0 \pm 0.2 \times 10^{-6}$	$8.8 \pm 1.0 \times 10^{-6}$
ET-637-OBu	OH	$7.1 \pm 0.8 \times 10^{-8}$	$3.5 \pm 0.4 \times 10^{-7}$	$7.8 \pm 0.8 \times 10^{-7}$
ET-637-OBu-C21(H)	H	$2.3 \pm 0.2 \times 10^{-5}$	$1.4 \pm 0.1 \times 10^{-6}$	$2.4 \pm 0.3 \times 10^{-5}$
ET-594	OH	$1.2 \pm 0.3 \times 10^{-7}$	$7.5 \pm 0.6 \times 10^{-7}$	$2.3 \pm 0.2 \times 10^{-6}$
ET-596	H	$2.9 \pm 0.3 \times 10^{-6}$	$1.3 \pm 0.2 \times 10^{-6}$	$4.1 \pm 0.6 \times 10^{-6}$

The presence of OH or H at C-21 is indicated. Values are IC_{50} in M and are shown as mean values ± SD of six independent experiments.

lack of the C21-OH group in the already poorly active ET-594 compound has little effect on the cytotoxic activity in both HeLa and A549 cells (Table 2).

Discussion

To our knowledge, this is the first structure-activity study carried out with trabectedin analogs. The data reported here demonstrate that the DNA interacting ability of trabectedin is dramatically dependent on the C21-OH, and changes in the C moiety of the trabectedin molecule affect DNA binding affinity. Thus, ET-745, lacking the C21-OH, does not bind to DNA, and the other analogs basically recognize the same sites as trabectedin in DNA, preferentially GC-enriched sequences, but with a lower affinity. Overall, the sequence selectivity of trabectedin is essentially maintained with the different analogs, although, in all cases, the modification of the C domain has a modest but noticeable effect on DNA sequence recognition. For example, trabectedin binds more strongly to CGG sites compared to GCG, whereas the opposite was observed with the N-acetyl analog ET-637. According to NMR and molecular modeling studies, the C domain of trabectedin is oriented perpendicularly to the A-B core and protrudes outside the double helix [21, 22]; however the 7′-methoxy group on the tetrahydroisoquinoline C domain could putatively establish contact with a DNA base. Thus, modification of the C domain might modulate the DNA binding capacity of the drug, either via the loss of a direct contact or as a result of structural perturbation. Another possibility is that the C domain markedly affects the kinetics of the bonding reaction and/or the intrinsic stability of the alkylated complex. We have found here that all of the trabectedin analogs studied are able to induce both cell cycle arrest and apoptosis in a dose-dependent way, suggesting that both biological responses are mediated through the extension at which the trabectedin target(s) is(are) affected. The fact that ET-745, unable to bind DNA, can induce cell cycle arrest and apoptosis in HL-60 and HeLa cells, although to a much smaller efficiency than other DNA binding analogs, suggests the existence of an additional non-DNA target for trabectedin that eventually would signal downstream events, leading to cell cycle arrest or apoptosis. However, this putative, additional non-DNA target seems to be more efficiently affected through the formation of a ternary complex together with the drug and DNA. The finding that all of the C21-OH-deficient compounds, which are thereby unable to bind to DNA, show a poor cytotoxic activity suggests that interaction of trabectedin with DNA is required to mount an optimum biological response. It is interesting to note that ET-637 and ET-594 show practically identical DNA binding properties but have very different cytotoxic and transcriptional profiling activities, further suggesting that additional non-DNA targets can play a role in trabectedin antitumor action. These data suggest that DNA is a necessary condition, but not sufficient, to raise an effective apoptotic response. However, it cannot be ruled out at present that ET-594 might be sequestered by cell proteins, preventing its interaction with DNA and thus leading to a minor biological response. On the other hand, the earlier finding that protein synthesis was required for trabectedin-induced cell cycle arrest [16] suggests the involvement of a protein in the action of this drug. Taken together, we can envision a hypothetic model for the action of trabectedin that can be used as a working hypothesis. This model would involve the existence of two targets for trabectedin, namely, DNA and a non-DNA target, likely a protein located close to DNA. Trabectedin binding to DNA would facilitate and stabilize the interaction with this putative, second non-DNA target, leading to the formation of a ternary complex that eventually would trigger apoptosis or cell cycle arrest. Failure to bind DNA would lead to a much less effective response. Interestingly, trabectedin antitumor action is dependent on transcription when used at low concentration [16], and we have found that the analogs herein studied promote gene regulation patterns that correlate very well with their corresponding cytostatic and cytotoxic actions. A number of DNA repair genes, including *XPC*, *GADD45*, and *DDB2*, were upregulated by the biologically active analogs, but not by the rather inactive analogs. This differential expression of DNA repair genes could play an important role in the antitumor action of this drug. In this regard, trabectedin-induced tumor killing has been proposed to be dependent upon transcription-coupled nucleotide-excision repair [15]. The fact that trabectedin analogs unable to bind DNA can still induce cell cycle arrest and apoptosis in a number of tumor cell lines, although with a much lower efficiency than DNA-interacting analogs, suggests that the interaction of trabectedin with a putative non-DNA target can lead to cytotoxicity. This opens the possibility of searching for non-DNA-interacting analogs that can induce apoptosis without affecting the rather non-specific DNA target.

It is interesting to note that the natural product saframycin A shows remarkable structural similarities, as well as a similar cytotoxic activity (in the nM range), to trabectedin. The analysis of the genetic responses to saframycin A treatment showed that this drug did not affect the expression of known DNA-damage repair genes, suggesting that the primary mechanism of action of saframycin A may not involve known DNA-damage pathways [23]. However, our proposed model for the formation of a protein-DNA-trabectedin ternary complex has found experimental support with the recent findings by Xing et al. [24], who have shown that saframycin A forms ternary complexes with GAPDH and DNA and have identified GAPDH as a protein target of saframycin A.

Significance

To our knowledge, the present work represents the first structure-activity study with trabectedin analogs. This has led us to conclude that: (1) the C21-hydroxyl group is both essential for DNA binding and is important for an optimum biological activity; (2) variations in the C domain of the trabectedin molecule result in modifications in both biological activity and DNA binding capacity; and (3) trabectedin interaction with DNA is necessary, but not sufficient, to mount an optimum biological response. Gel shift and DNase I footprinting assays with distinct DNA sequences showed that the analogs ET-637 and ET-594, with different modifications at the C domain of the trabectedin molecule, displayed similar DNA binding activities, but had very different biological responses. Our data suggest that trabectedin interacts with both DNA and an additional non-DNA target to raise a potent antitumor response, likely via its C domain. This latter interaction with a putative non-DNA target could be greatly favored by the formation of trabectedin-DNA complexes. The C domain of trabectedin seems to play a pivotal role, possibly by promoting molecular talk between DNA and the additional, yet unidentified target. The interaction of trabectedin with this target could mount a graded response, cell cycle arrest, or apoptosis. Although some analogs showed similar DNA binding activities but distinct biological responses, assessed as cell cycle arrest and induction of apoptosis, we found a remarkable correlation between biological responses and changes induced in gene expression by the distinct trabectedin analogs. This can provide potential clinical response markers on the basis of gene expression changes in tumors. Our present studies might set a framework for the design of additional trabectedin analogs with improved antitumor efficacy and/or reduced toxicity.

Experimental Procedures

Materials

Trabectedin and its analogs were provided by PharmaMar (Colmenar Viejo, Madrid, Spain). The synthesis of trabectedin and its analogs ET-745, ET-637, and ET-594 has been recently reported [25]. The chemical synthesis of the other analogs used in the present study will be described elsewhere.

DMEM and RPMI-1640 culture media, fetal calf serum (FCS), antibiotics, and L-glutamine were purchased from Life Technologies, Inc. (Gaithersburg, MD). Mouse monoclonal antibody C2.10 against human PARP was purchased from Enzyme Systems Products (Livermore, CA). Anti-JNK1 (C-17) rabbit polyclonal antibody; mouse monoclonal anti-phospho-JNK antibody G-7, raised against a peptide corresponding to a short amino acid sequence containing phosphorylated Thr-183 and Tyr-185 of human JNK; mouse monoclonal anti-phospho-ERK antibody E-4, raised against a short amino acid sequenced containing phosphorylated Tyr-204 of human ERK (identical to both ERK1 and ERK2); and mouse monoclonal anti-ERK-2 antibody D-2, raised against a peptide mapping at the carboxy terminus of human ERK-2, were purchased from Santa Cruz Biotechnology (Santa Cruz, CA). Acrylamide, bisacrylamide, ammonium persulfate, and N,N,N′,N′-tetramethylethylenediamine were purchased from Bio-Rad (Richmond, CA). All other chemicals were purchased from Merck (Darmstadt, Germany) or Sigma.

Cell Culture

The human acute myeloid leukemia HL-60 cell line and the human lung carcinoma A549 cell line were grown in RPMI-1640 supplemented with 10% (v/v) heat-inactivated FCS, 2 mM L-glutamine, 100 U/ml penicillin, 100 μg/ml streptomycin, and 24 μg/ml gentamicin. The human epitheloid cervix carcinoma HeLa cell line was grown in DMEM culture medium supplemented with FCS and antibiotics as described above. Cells were incubated at 37ºC in a humidified atmosphere of 5% CO_2/95% air.

Cell Growth Inhibition Assay

Exponentially growing HeLa and A549 cells were seeded at 1.5×10^3/100 μl and 3×10^3/100 μl per well, respectively, in 96-well, flat-bottomed microtiter plates, and they were incubated at 37ºC in a humidified atmosphere of 5% CO_2/95% air for 24 hr to let the cells attach to the plates. HL-60 cells were seeded at 5×10^3 (100 μl) cells per well. Then, cells were incubated with different drug concentrations at 37ºC under the 5% CO_2/95% air atmosphere for 72 hr. Cell proliferation was quantified by using the XTT (sodium 3′-[1-(phenylamino-carbonyl)-3,4-tetrazolium]-bis (4-methoxy-6-nitro) benzene sulfonic acid hydrate) cell proliferation kit (Roche Molecular Biochemicals, Mannheim, Germany) according to the manufacturer's instructions. Briefly, a freshly prepared mixture solution of XTT labeling reagent and PMS (N-methyl dibenzopyrazine methyl sulfate) electron coupling reagent was added to each well in the amount of 50 μl. The resulting mixtures were further incubated for 4 hr in a humidified atmosphere (37ºC, 5% CO_2), and the absorbance of the generated formazan product was measured with a microtiter plate reader at a test wavelength of 490 nm and a reference wavelength of 655 nm. IC_{50} (50% inhibitory concentration) was then calculated as the drug concentration causing 50% inhibition in cell proliferation.

Apoptosis

The induction of apoptosis was monitored by fluorescence flow cytometry as the appearance of the sub-G_1 peak in cell cycle analysis [16] by using a Becton Dickinson FACSCalibur flow cytometer (San Jose, CA). Quantitation of apoptotic cells was calculated as the percentage of cells in the sub-G_1 region (hypodiploidy) in cell cycle analysis.

Western Blot Analysis

About 10^7 cells were pelleted by centrifugation, washed with PBS, lysed, and subjected to Western blot analysis as described previously [26]. Signals were developed by using an enhanced chemiluminescence (ECL) detection kit (Amersham Biosciences, Aylesbury, UK). Immunoblotting with the mouse monoclonal anti-β-actin antibody AC15 (Sigma) was used as an internal loading control.

Thermal Denaturation Studies

The 16 bp double-stranded oligonucleotide (5′-CTTTAGTGAGGGT TAA-3′ and its complementary strand, 20 μM) was incubated alone (control *Tm*) or with 1 or 2 μM (drug:base ratio of 0.05 or 0.1) of the various molecules in 1 ml BPE buffer (6 mM Na_2HPO4, 2 mM NaH_2PO_4, 1 mM EDTA [pH 7.1]). The absorbance at 260 nm was measured every min over the range of 20ºC–90ºC with an increment of 1ºC per min in 1 cm path length quartz cells by using a Uvikon 943

spectrophotometer thermostated with a Neslab RTE111 cryostat. The *Tm* values were determined from the first derivatives plots.

Gel Shift Experiments

These assays were carried out on agarose and acrylamide gels. A 2900 bp DNA fragment was obtained from BamHI digestion of plasmid pLAZ. DNA (130 ng) was incubated with the various drugs at 1–50 μM for 1 hr at room temperature in the binding buffer containing 10 mM Tris, 10 mM NaCl (pH 7.0) prior to electrophoresis on 1% agarose gels (poststained with ethidium bromide). A 56 bp DNA fragment was 3′ end labeled by using α-[^{32}P]-dATP and AMV reverse transcriptase for 2 hr at 37ºC prior to being purified on a 10% native polyacrylamide gel as described in "DNase I Footprinting." To prepare the footprint oligonucleotide and the triplet-containing double-stranded DNA targets for mobility shift assays in acrylamide gels, a synthetic 16-mer oligonucleotide d(CTTTAGT GAGGGTTAA) or various triplet-containing oligonucleotides and their respective complementary strands were mixed at a 1:1 ratio, heated to 75ºC, and slowly cooled to form duplexes, which were then labeled at the 5′ end by using γ-[^{32}P]-ATP and T4 polynucleotide kinase. Labeled DNA was then purified by electrophoresis on a 10% (w/v) polyacrylamide gel to remove the excess radioactive nucleotide, cut out of the gel, and eluted overnight in 10 mM Tris (pH 8.0), 1 mM EDTA, 100 mM NaCl. Samples were then ethanol precipitated, and the DNA pellet was dissolved in H_2O. The typical crosslinking reaction consisted of incubating 20,000 cpm radiolabeled DNA with the test drug (15 μM each) for 1 hr at 37ºC in 20 μl binding buffer (10 mM Tris [pH 7.0], 10 mM NaCl). After the addition of 5 μl of a 50% glycerol solution containing tracking dyes, DNA samples were resolved by electrophoresis under nondenaturing conditions in 10% polyacrylamide gels for about 4 hr at 300V at room temperature in TBE buffer (89 mM Tris base, 89 mM boric acid, 2.5 mM Na_2EDTA [pH 8.3]). Gels were transferred to Whatman 3 MM paper, dried under vacuum at 80ºC, and then analyzed on a Molecular Dynamics 445SI phosphorimager (Molecular Dynamics, Sunnyvale, CA).

DNase I Footprinting

The pTUC plasmid and the pBS plasmid were digested with PvuII-EcoRI restriction enzymes, and the resulting 176 bp or 265 bp fragments, respectively, were labeled at the 3′ end (EcoRI site) with α-[^{32}P]-dATP and AMV reverse transcriptase. Electrophoresis on a nondenaturing 6% (w/v) polyacrylamide gel was performed to remove the excess radioactive nucleotide, and the desired 3′ end-labeled product was cut out from the gel and eluted overnight in 10 mM Tris (pH 8.0), 1 mM EDTA, 100 mM NaCl. The DNA fragment was then ethanol precipitated, and the DNA pellet was resuspended in H_2O. For the footprinting reactions, samples (3 μl) of the labeled DNA fragment were incubated with 5 μl of the buffered solution containing the various compounds at the indicated concentrations. After 15 min of incubation at room temperature, the digestion was initiated by the addition of 2 μl of a DNase I solution (final concentration 0.01 U/ml). After 3 min of incubation, the reaction was stopped by freeze drying and lyophilization of the samples. The resulting DNA pellet was resuspended in 5 μl of an 80% formamide solution containing tracking dyes, heated at 90ºC for 4 min, and chilled in ice for 4 min prior to electrophoresis on polyacrylamide gels under denaturating conditions (8% acrylamide containing 8 M urea) in TBE buffer. After electrophoresis, gels were soaked in 10% acetic acid for 10 min, dried, and analyzed as described above.

Affymetrix Microarray Analysis

We analyzed RNA samples prepared from three independent experiments for each experimental condition, namely, untreated and treated with distinct trabectedin analogs at 3 nM. Total RNA was isolated by using a RNeasy kit (Qiagen, Valencia, CA), and double-stranded cDNA was synthesized from 15 μg total RNA by means of the SuperScript double-stranded cDNA synthesis kit (Invitrogen, San Diego, CA) with oligo(dT)$_{24}$ primer containing T7 RNA polymerase promoter. In vitro transcription was carried out as previously described [16]. Microarray RNA analysis was performed according to the manufacturer's protocol with the Human Genome U133A GeneChip (Affymetrix, Santa Clara, CA). Chips were stained and washed with an Affymetrix fluids station and by following the manufacturer's protocol. Chips were scanned with the HP Agilent GeneArray Scanner, and values were normalized to a baseline array with overall median intensity and were analyzed with the Affymetrix Microarrays Suite 5.0 (MAS5.0) and GeneSpring 5.0 programs. Arrays were scaled to an average intensity of 100 by using 1 as the normalization factor and were analyzed independently by using the untreated control samples as baselines. Only genes classified as "present" were considered.

Statistical Analyses

Unless otherwise indicated, the results given are the mean (±SD) of the number of experiments indicated.

Acknowledgments

This work was supported by grants from Fondo de Investigación Sanitaria and European Commission (FIS04/0843, FIS02/1199), Fundación de Investigación Médica Mutua Madrileña (FMM), Fundación "la Caixa" (BM05-30-0), Junta de Castilla y León (CSI04A05) (to F.M.), The Institut de Recherches sur le Cancer de Lille (IRCL), the Ligue Nationale contre le Cancer, comité du Nord (to C.B. and to M.-H.D.-C.), The Foundation pour la Recherche Medical (post-doctoral fellowship to M.-H.D.-C.), and by grants from PharmaMar. C.G. was supported by the Ramón y Cajal Program from the Ministerio de Educación y Ciencia of Spain.

Received: January 10, 2005
Revised: July 20, 2005
Accepted: August 10, 2005
Published: November 18, 2005

References

1. Li, W.W., Takahashi, N., Jhanwar, S., Cordon-Cardo, C., Elisseyeff, Y., Jimeno, J., Faircloth, G., and Bertino, J.R. (2001). Sensitivity of soft tissue sarcoma cell lines to chemotherapeutic agents: identification of ecteinascidin-743 as a potent cytotoxic agent. Clin. Cancer Res. *7*, 2908–2911.
2. Erba, E., Bergamaschi, D., Bassano, L., Damia, G., Ronzoni, S., Faircloth, G.T., and D'Incalci, M. (2001). Ecteinascidin-743 (ET-743), a natural marine compound, with a unique mechanism of action. Eur. J. Cancer *37*, 97–105.
3. Aune, G.J., Furuta, T., and Pommier, Y. (2002). Ecteinascidin 743: a novel anticancer drug with a unique mechanism of action. Anticancer Drugs *13*, 545–555.
4. Scotto, K.W. (2002). ET-743: more than an innovative mechanism of action. Anticancer Drugs *13* (*Suppl 1*), S3–S6.
5. van Kesteren, C., de Vooght, M.M., Lopez-Lazaro, L., Mathot, R.A., Schellens, J.H., Jimeno, J.M., and Beijnen, J.H. (2003). Yondelis (trabectedin, ET-743): the development of an anticancer agent of marine origin. Anticancer Drugs *14*, 487–502.
6. Pommier, Y., Kohlhagen, G., Bailly, C., Waring, M., Mazumder, A., and Kohn, K.W. (1996). DNA sequence- and structure-selective alkylation of guanine N2 in the DNA minor groove by ecteinascidin *743*, a potent antitumor compound from the Caribbean tunicate *Ecteinascidia turbinata*. Biochemistry *35*, 13303–13309.
7. Gago, F., and Hurley, L.H. (2003). Devising a structural basis for the potent cytotoxic effects of ecteinascidin 743. In Small Molecule DNA and RNA Binders, Volume 2, M. Demeunynck, C. Bailly, and W.D. Wilson, eds. (Weinheim, Germany: Wiley-VCH), pp. 643–675.
8. Takebayashi, Y., Pourquier, P., Yoshida, A., Kohlhagen, G., and Pommier, Y. (1999). Poisoning of human DNA topoisomerase I by ecteinascidin *743*, an anticancer drug that selectively alkylates DNA in the minor groove. Proc. Natl. Acad. Sci. USA *96*, 7196–7201.
9. Minuzzo, M., Marchini, S., Broggini, M., Faircloth, G., D'Incalci, M., and Mantovani, R. (2000). Interference of transcriptional activation by the antineoplastic drug ecteinascidin-743. Proc. Natl. Acad. Sci. USA *97*, 6780–6784.
10. Garcia-Rocha, M., Garcia-Gravalos, M.D., and Avila, J. (1996). Characterisation of antimitotic products from marine organisms that disorganise the microtubule network: ecteinascidin *743*, isohomohalichondrin-B and LL-15. Br. J. Cancer *73*, 875–883.

11. van Kesteren, C., Cvitkovic, E., Taamma, A., Lopez-Lazaro, L., Jimeno, J.M., Guzman, C., Math t, R.A., Schellens, J.H., Misset, J.L., Brain, E., et al. (2000). Pharmacokinetics and pharmacodynamics of the novel marine-derived anticancer agent ecteinascidin 743 in a phase I dose-finding study. Clin. Cancer Res. *6*, 4725–4732.
12. Taamma, A., Misset, J.L., Riofrio, M., Guzman, C., Brain, E., Lopez Lazaro, L., Rosing, H., Jimeno, J.M., and Cvitkovic, E. (2001). Phase I and pharmacokinetic study of ecteinascidin-743, a new marine compound, administered as a 24-hour continuous infusion in patients with solid tumors. J. Clin. Oncol. *19*, 1256–1265.
13. Ryan, D.P., Puchalski, T., Supko, J.G., Harmon, D., Maki, R., Garcia-Carbonero, R., Kuhlman, C., Winkelman, J., Merriam, P., Quigley, T., et al. (2002). A phase II and pharmacokinetic study of ecteinascidin 743 in patients with gastrointestinal stromal tumors. Oncologist *7*, 531–538.
14. Damia, G., Silvestri, S., Carrassa, L., Filiberti, L., Faircloth, G.T., Liberi, G., Foiani, M., and D'Incalci, M. (2001). Unique pattern of ET-743 activity in different cellular systems with defined deficiencies in DNA-repair pathways. Int. J. Cancer *92*, 583–588.
15. Takebayashi, Y., Pourquier, P., Zimonjic, D.B., Nakayama, K., Emmert, S., Ueda, T., Urasaki, Y., Kanzaki, A., Akiyama, S.I., Popescu, N., et al. (2001). Antiproliferative activity of ecteinascidin 743 is dependent upon transcription-coupled nucleotide-excision repair. Nat. Med. *7*, 961–966.
16. Gajate, C., An, F., and Mollinedo, F. (2002). Differential cytostatic and apoptotic effects of ecteinascidin-743 in cancer cells. Transcription-dependent cell cycle arrest and transcription-independent JNK and mitochondrial mediated apoptosis. J. Biol. Chem. *277*, 41580–41589.
17. Corey, E.J., Gin, D.Y., and Kania, R.S. (1996). Enantioselective total synthesis of ecteinascidin 743. J. Am. Chem. Soc. *118*, 9202–9203.
18. Cuevas, C., Perez, M., Martin, M.J., Chicharro, J.L., Fernandez-Rivas, C., Flores, M., Francesch, A., Gallego, P., Zarzuelo, M., de La Calle, F., et al. (2000). Synthesis of ecteinascidin ET-743 and phthalascidin Pt-650 from cyanosafracin B. Org. Lett. *2*, 2545–2548.
19. Martinez, E.J., Owa, T., Schreiber, S.L., and Corey, E.J. (1999). Phthalascidin, a synthetic antitumor agent with potency and mode of action comparable to ecteinascidin 743. Proc. Natl. Acad. Sci. USA *96*, 3496–3501.
20. Moore, B.M., Seaman, F.C., Wheelhouse, R.T., and Hurley, L.H. (1998). Mechanism of the catalytic activation of eceteinascidin 743 and its subsequent alkylation of guanine N2. J. Am. Chem. Soc. *120*, 2490–2491.
21. Moore, B.M., Seaman, F.C., and Hurley, L.H. (1997). NMR-based model of an ecteinascidin 743-DNA adduct. J. Am. Chem. Soc. *23*, 5475–5476.
22. Seaman, F.C., and Hurley, L.H. (1998). Molecular basis for the DNA sequence selectivity of ecteinascidin 736 and 743: evidence for the dominant role of direct readout via hydrogen bonding. J. Am. Chem. Soc. *120*, 13028–13041.
23. Plowright, A.T., Schaus, S.E., and Myers, A.G. (2002). Transcriptional response pathways in a yeast strain sensitive to saframycin a and a more potent analog: evidence for a common basis of activity. Chem. Biol. *9*, 607–618.
24. Xing, C., LaPorte, J.R., Barbay, J.K., and Myers, A.G. (2004). Identification of GAPDH as a protein target of the saframycin antiproliferative agents. Proc. Natl. Acad. Sci. USA *101*, 5862–5866.
25. Menchaca, R., Martinez, V., Rodriguez, A., Rodriguez, N., Flores, M., Gallego, P., Manzanares, I., and Cuevas, C. (2003). Synthesis of natural ecteinascidins (ET-729, ET-745, ET-759B, ET-736, ET-637, ET-594) from cyanosafracin B. J. Org. Chem. *68*, 8859–8866.
26. Gajate, C., Santos-Beneit, A.M., Macho, A., Lazaro, M., Hernandez-De Rojas, A., Modolell, M., Munoz, E., and Mollinedo, F. (2000). Involvement of mitochondria and caspase-3 in ET-18-OCH(3)-induced apoptosis of human leukemic cells. Int. J. Cancer *86*, 208–218.